Journal of Asian Concrete Federation
Vol. 7, No. 2, pp. 33-45, Dec. 2021
ISSN 2465-7964 / eISSN 2465-7972
DOI http://dx.doi.org/10.18702/acf.2021.12.7.2.33

Electrochemical and microscopic analysis on corrosion behavior of steel bars in slag/fly ash-cement paste subjected to seawater attack

Shuai Zou, Xiao-Bao Zuo, Xiangnan Li, Jianzhuang Xiao*

(Received: July 07, 2021; Accepted: October 29, 2021; Published online: December 30, 2021)

Abstract: A series of corrosion experiments of cement paste-steel bar specimens with different contents of slag and fly ash were performed to investigate the influence of slag/fly ash on the corrosion behavior of steel bars in concrete under seawater. In this investigation, the corrosion behavior of specimen was electrochemically monitored by open-circuit potential (OCP), Tafel polarization (TP) and electrochemical impedance spectra (EIS). Meanwhile, SEM/EDS and XRD were applied to microscopically analyze the microstructure deterioration of materials. Results showed that, replacing cement with slag/fly ash caused a decrease in $Ca(OH)_2$ as well as an increase in C-S-H gel and Friedel's salt in concrete, which can improve the chloride-solidification ability and slow down the chloride diffusion in concrete by both physical adsorption and chemical binding, and thereafter promoting the corrosion resistance of steel bars in concrete in marine environment. Compared to slag, the equal replacing content of fly ash can contribute to a better improving effect on the corrosion resistance of reinforced concrete in marine environment. In this study, a replacement of cement by 20% slag+20% fly ash led to an optimum improving effect on its corrosion resistance. In addition, the results also indicate that the corrosion of reinforced concrete caused by seawater attack does not occur at a uniform rate, but it can firstly maintain a long-term uncorroded state, and then develops rapidly after pitting corrosion occurs.

Keywords: Cement paste; Slag/Fly ash; Steel bar Corrosion; Chloride attack; Electrochemical; SEM/XRD.

1. Introduction

Chloride attack has been considering as one of the major causes for the corrosion of steel bar in concrete and the durability deterioration of structures in marine environment [1,2]. It is well known that steel bar in concrete is normally in passive state due to the high alkaline environment induced by cement hydration [3,4]. However, the steel bar will depassivate and corrode when chloride ions in seawater penetrate through the concrete cover to the surface of steel and reach a certain critical level, namely chloride threshold value (CTV) [5–7]. Furthermore, the volume expansion caused by continuous steel corrosion can result in the cracking of concrete in the cover, which will accelerate the penetration of chloride ions and finally deteriorate the performance of reinforced concrete, thereafter reducing the bearing capacity and shortening the service life of concrete structures in marine environment [8–10]. Thus, in order to improve the durability of concrete structures in marine environment, the research on the corrosion behavior and anti-corrosion methods of steel bar in reinforced concrete is significant.

As reported, several methods have been investigated to improve the durability of reinforced concrete subjected to the attack of seawater, including increasing concrete cover, coated rebar, cathodic protection, corrosion inhibitors, utilizing stainless steel, adding mineral admixtures, etc. [11,12]. Among them, the application of mineral admixtures, for example, the replacement of OPC with slag and fly ash has gained more and more attentions over the past decade [13,14]. This is partly because the production of Ordinary Portland Cement (OPC) was reported to contribute about 6-8% of the total global carbon dioxide (CO_2) emission [15]. Under the green and sustainable development background, alternative materials like slag and fly ash are preferred to replace OPC to release the pollution pressure of the construction industry.

Corresponding author Jianzhuang Xiao *is a professor and head of Department of Structural Engineering, College of Civil Engineering, Tongji University, Shanghai 200092, China and Key Laboratory of Performance Evolution and Control for Engineering Structures of Ministry of Education, Tongji University, Shanghai 200092, China;*

Shuai Zou *was a Master student of Department of Civil Engineering, School of Science, Nanjing University of Science & Technology, Nanjing, 210094, China*

Xiaobao Zuo *is a professor of Department of Civil Engineering, School of Science, Nanjing University of Science & Technology, Nanjing, 210094, China*

Xiangnan Li *is a PhD student of Department of Civil Engineering, School of Science, Nanjing University of Science & Technology, Nanjing, 210094, China*

On the other hand, incorporating slag/fly ash into reinforced concrete has been proved to be low production cost and good anti-corrosion performance [16,17]. The research by Sun et al.[18] pointed out that the pozzolanic reaction of slag and fly ash can change the microstructure and phase composition of concrete, which exhibited significant benefits in improving the corrosion resistance of reinforced concrete in marine environments. Similar result was also reported by Jau et al. [19] with the investigation on the mechanical properties and durability of slag-cement concrete immersed into sea water. And the optimum corrosion resistance was found to be a substitution of 20–30% cement by slag. The research of Boga et al. [20] indicated that corrosion-resistant concrete can be prepared by using slag mineral admixture at the ratio of 25%. However, Mangat et al. [21] stated that the replacement of cement by up to 40% slag has no significant influence on rebar corrosion. Meanwhile, in the work of Lekatou et al. [22], the concrete electrolyte with fly ash content of 20% by weight led to the highest corrosion resistance. Nevertheless, the optimum replacing content of fly ash to cement when considering the improvement of corrosion resistance in reinforced concrete was shown to be in a range of 10-60% by weight in other investigations [23,24].

From the literature review, it can be found that the alternative dosage of slag/fly ash to cement were discrete when considering the optimum improving effect on the corrosion resistance of reinforced concrete in marine environment. This can be explained by the fact that various accelerating and simulating methods were usually used in the durability experiment because of its long period feature and difficulty in direct detection and quantitative judgment on the corrosion degree of steel bar in concrete. As reported, the electrochemical measurement, combined with microscopic analysis by SEM/EDS/XRD, was an effective approach for dynamically and accurately monitoring the corrosion behavior of steel bars in concrete [25,26]. Goyal et al. [27] has used the potentials obtained by Tafel polarization (TP) to predict the corrosion rate of steel bars in cathodically protected concrete. In Subramaniam's research [28], the TP response was utilized to evaluate the corrosion rate of steel bars in cracked concrete. Additionally, the electrochemical impedance spectrum (EIS) has also been applied by Ribeiro [29] to monitor the corrosion behavior of reinforced concrete. Thus, by using electrochemical measurements and utilizing the seawater of the East China Sea, not only the corrosion of steel bars can be dynamically and accurately monitored, but the penetration of chloride ions in seawater from the concrete cover to the steel surface can also be simulated. In this way, a relatively more accurate method is provided to research the influence of slag and fly ash on the corrosion behavior of reinforced concrete in marine environment.

In this study, the cement paste-steel (CPR) specimens with different contents of slag and fly ash were firstly prepared, and then, the prepared specimens were immersed in the seawater of the East China Sea to simulate the natural penetration of chloride ions in marine environment. Electrochemical measurements, such as open-circuit potential (OCP), TP and EIS, were selected to dynamically monitor the specimens' corrosion behavior. Meanwhile, microscopic analysis, such as scanning electron microscopy (SEM) together with Energy Dispersive X-ray Spectroscopy (EDS) and X-ray diffraction (XRD) were used to investigate the specimens' microstructure and phase. The simultaneous studies on the electro- and micro- properties of the CPR specimens would be helpful for revealing the effect of slag/fly ash on corrosion behavior of reinforced concrete in marine environment.

2. Experiments

2.1 Materials

In this study, 52.5-grade OPC, grade blast furnace slag powder, and Class F fly ash were selected as cementitious materials. Their density and specific surface area are respectively 3100 kg/m^3, 2900 kg/m^3, and 2240 kg/m^3 as well as 350 m^2/kg, 435m^2/kg, and 454m^2/kg. The chemical compositions of cement, slag and fly ash are presented in Table 1.

Table 1 – Chemical composition of cement and slag (Mass content, %)

Material	SiO_2	Al_2O_3	CaO	MgO	SO_3	Fe_2O_3	K_2O	Na_2O	TiO_2
Cement	21.1	5.56	62.48	1.76	3.59	3.98	0.94	0.20	0.14
Slag	33.4	12.21	42.70	6.70	0.30	0.43	0.56	1.27	1.07
Fly ash	57.6	21.90	3.87	1.68	0.41	2.70	1.62	0.55	1.25

The steel bar with a tensile strength of 235 MPa and elastic modulus of 210 GPa was selected because of its smooth surface which is easy to form passive film. Also, its element composition is listed in Table 2.

Table 2 – Element composition of steel bar (Mass content, %)

Elements	C	S	P	Mn	Si	Fe
Contents(mass)	0.20	0.039	0.021	1.42	0.56	97.76

2.2 Specimens and chloride solution

Firstly, a batch of steel bars with length of 30 mm and diameter of 10 mm were prepared and successively cleaned up with the diluted hydrochloride acid, acetone, and pure water. And then, copper wire with length of 200 mm was welded into the steel bar's end. Secondly, two ends of the cylindrical steel bar were coated with epoxy resin and centered in PVC pipe with inner diameter of 6 mm. Mixed cement paste with different contents of slag and fly ash was injected into the space between PVC pipe and steel bar. After natural curing for 24 hours, the PVC pipe was removed, and the specimens were transported to the standard concrete curing box with temperature of 20 ± 2 °C and humidity of 95 ± 5% for further curing. Finally, two ends of the specimen were covered with epoxy resin after curing for 27 days, leaving its cylindrical surface with area of 9.42 cm^2 used as the corrosion surface. The prepared electrochemical specimen is shown in Fig. 2 and the related parameters are listed in Table 3. In the Table, CPR, SCPR2, SCPR4, FCPR1, FCPR2, FSCPR1, and FSCPR2 represent the specimens with 100% cement, 20% slag, 40% slag, 10% fly ash, 20% fly ash, 10% slag + 10% fly ash, 20% slay + 20% fly ash, respectively. Each group of the specimens was immersed in one container, and the ratio in volume between specimen and corrosion solution is 1: 50. A continuous immersion method of the specimens in seawater from East China Sea was carried out to simulate the natural penetration of chloride ion in marine environment.

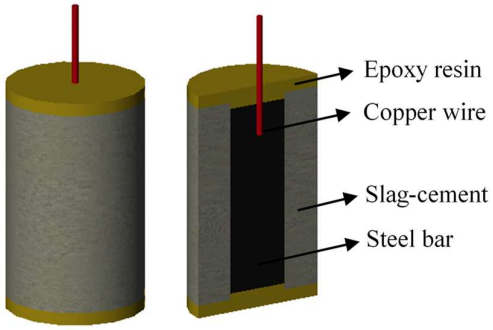

Fig. 1 – Schematic diagram of the electrochemical specimen

Table 3 – Mix ratio of electrochemical specimen and its soaking solution. (Mass content, %)

Specimen number	Protective layer thickness (mm)	Water-binder ratio	Mass fraction/%				Corrosion solution
			Cement	Slag	Fly ash	Water	
CPR	6	0.45	100	0	0	45	Seawater
SCPR2	6		80	20	0		
SCPR4	6		60	40	0		
FCPR1	6		90	0	10		
FCPR2	6		80	0	20		
FSCPR1	6		80	10	10		
FSCPR2	6		60	20	20		

Notes: Triplicate specimens were prepared for each case to ensure the reproducibility of results.

2.3 Test methods

2.3.1 Electrochemical tests

The electrochemical tests were performed at room temperature (25±2℃) in a conventional three-electrode system using PARSTAT 2273 electrochemical workstation [30]. The electrochemical specimen in Fig. 1, commercial saturated calomel electrode (SCE) and platinum electrode were used as working electrode, reference electrode and counter electrode, respectively. Fig. 2 shows the schematic diagram of the measurement setup. Using this electrochemical testing system, the EIS and TP were measured and recorded every 15 days. EIS measurement was performed at stable OCP by supplying sinusoidal voltage of ±10mV with its

frequency in a range of 10^{-2}~10^{6} Hz. Five data were recorded at every frequency order of magnitude. The TP measurement was performed by applying a potential ranged from -100 mV to +150 mV based on the corrosion potential (E_{corr}) with a scan rate of 0.1 mV/s. Moreover, the Tafel curve extrapolation method was utilized to obtain the corrosion current density (i_{corr}) which can describe the stability of passive film and judge the corrosion state of steel in concrete [31].

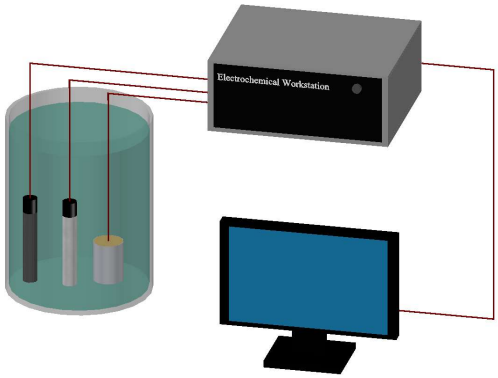

Fig. 2 – Schematic diagram of electrochemical measurements

SEM/EDS

After initial corrosion has been confirmed by the electrochemical measurements, specimens were broken to examine their microstructure morphology and chemical composition by the SEM with the EDS (FEI Quanta 250 FEG). The samples for microscopic analysis were prepared from the electrochemically corroded specimen, including steel bar sample and cement paste sample, as shown in Fig. 3.

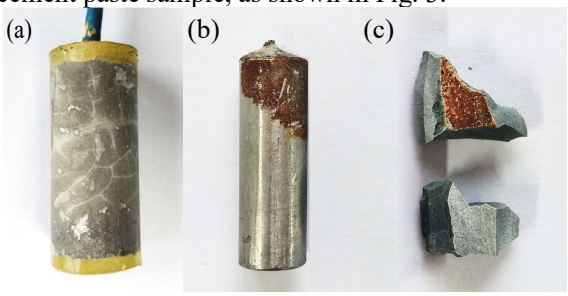

Fig. 3 – (a) Electrochemical specimen; (b) Steel sample; (c) Cement paste sample

XRD

The powdered sample from the cement paste layer was firstly dried in the vacuum box with a temperature of 105°C, and then its phase composition was analyzed by using the Brucker X-ray diffractometer with the LynxEye array detector [32]. Its working voltage and current were 40 kV and 40 mA, respectively, with a scanning rate of 0.15 second per step and a step size of 0.02° ranging from 10° to 80° (2θ).

3. Results and discussion

3.1 Open-circuit potential (OCP)

Fig. 4 presents the time-varying OCP of specimens with different slag and fly ash contents. It can be seen from the figure that, the initial OCPs of CPR, SCPR2, SCPR4, FCPR1, FSCPR1, FCPR2 and FSCPR2 were -182.2, -169.1, -172.3, -148.6, -235.3, -223.0 and -207.8 mV *vs*. SCE, respectively. Based on the ASTM C876 criterion [33], the judgment standard of OCP for the initial corrosion state is less than -350 mV *vs*. SCE, indicating that no corrosion happened on these specimens during the initial stage of immersion [34]. Subsequently, the specimens' OCPs exhibited different changes with immersion time. As for CPR, its OCPs remained stable during the first 120 days of immersion, and then, negatively shifted from -331.1 mV *vs*. SCE on the 135th day to -593.7 mV *vs*. SCE on the 150th day, and finally stabilized again. But for SCPR2, SCPR4, FCPR1, FSCPR1, FCPR2 and FSCPR2, their OCPs have always been fluctuating around the initial values until the 300th, 360th, 390th, 450th, 510th and 600th day, and then shifted to around -600 mV *vs*. SCE on the 360th, 420th, 450th, 510th, 600th and 690th day, respectively. These indicate that the CPR corroded on the 150th day, while the SCPR2, SCPR4, FCPR1, FSCPR1, FCPR2 and FSCPR2 reached the corrosion state after immersion in the seawater for 360, 420, 450, 510, 600 and 690 days, respectively. Thus, the equivalent replacement of cement with slag and fly ash can effectively improve the corrosion resistance of reinforced concrete in marine environment. Moreover, compared to slag, the equal replacing content of fly ash contributes to a better improving effect on the corrosion resistance.

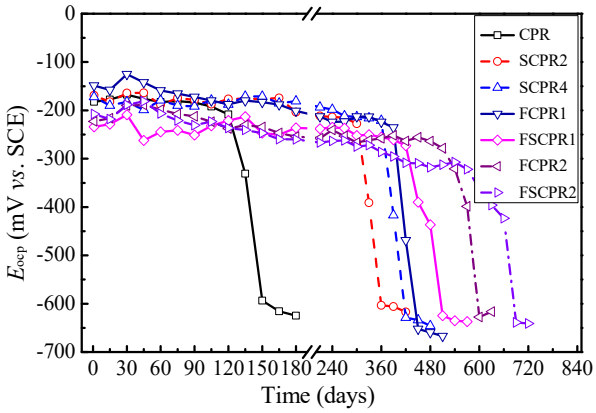

Fig. 4 – Time-varying OCP of CPR, SCPR2 and SCPR4 under seawater

3.2 Tafel polarization (TP)

Fig. 5 shows the time-varying TP and corrosion

current density (i_{corr}) curves of CPR, SCPR2, SCPR4, FCPR1, FCPR2, FSCPR1 and FSCPR2. It can be found from the figure that different specimens showed similar changes in their TP and i_{corr} curves during the immersion. More specifically, the corrosion potential (E_{corr}) in TP curves of these specimens firstly stabilized in the range of -0.15 ~ -0.25 V, and eventually moved negatively to the range of -0.55 ~ -0.65 V. Generally, a higher E_{corr} and a lower i_{corr} represent a better corrosion resistance on the surface of steel bars [35]. Thus, the change of these specimens' E_{corr} indicates their gradually corrosion process in the seawater.

In order to further analyze the corrosion behavior of these specimens under marine environment, the i_{corr} of each specimen was obtained by extrapolation method of TP curves. It can be observed from Fig. 6(h) that, the i_{corr} of CPR, SCPR2, SCPR4, FCPR1, FSCPR1, FCPR2 and FSCPR2 kept stable at a low level (around 0.1 $\mu A.cm^{-2}$) during their immersion days of 120, 300, 360, 390, 450, 540 and 630 days, respectively. And then, their i_{corr} increased to a high level (much higher than 0.2 $\mu A.cm^{-2}$) on the 150th, 360th, 420th, 450th, 510th, 600th and 690th day, respectively. According to Clear criterion [36], the critical corrosion current density for the corrosion of steel bars in concrete is 0.2 $\mu A.cm^{-2}$. So, the steel bar in CPR was in a corrosion state after immersion for 150 days in seawater, while the steel bar in SCPR2, SCPR4, FCPR1, FCPR2 FSCPR1, and FSCPR2 took 360, 420, 450, 510, 600 and 690 days to reach the corrosion state, respectively. The results indicated that the equivalent replacement of cement with slag and fly ash can significantly improve the corrosion resistance of reinforced concrete, and the equal replacement of fly ash had better improving effect than that of slag.

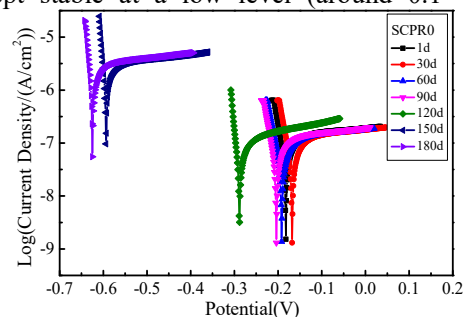

(a) CPR

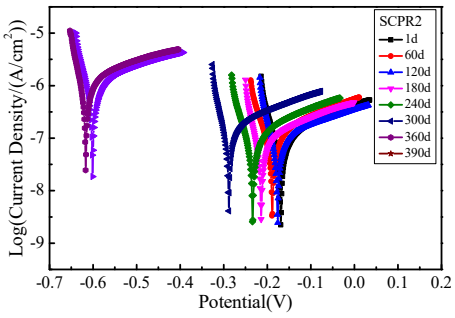

(b) SCPR2

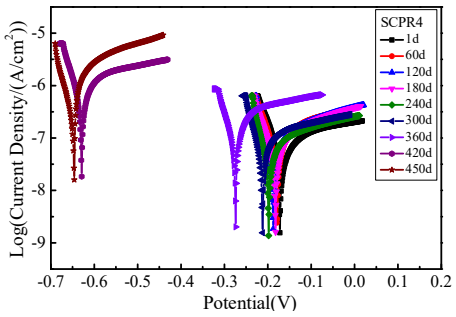

(c) SCPR4

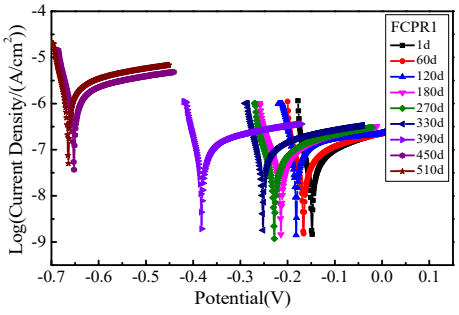

(d) FCPR1

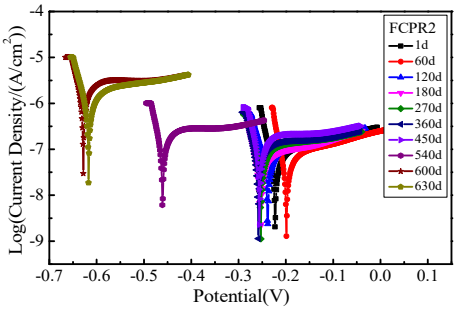

(e) FCPR2

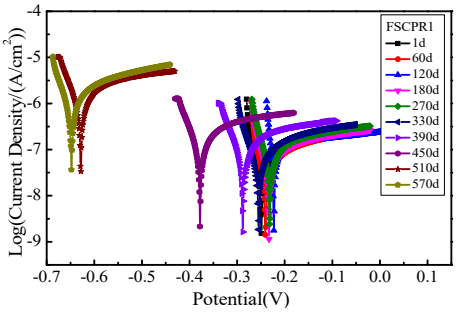

(f) FSCPR1

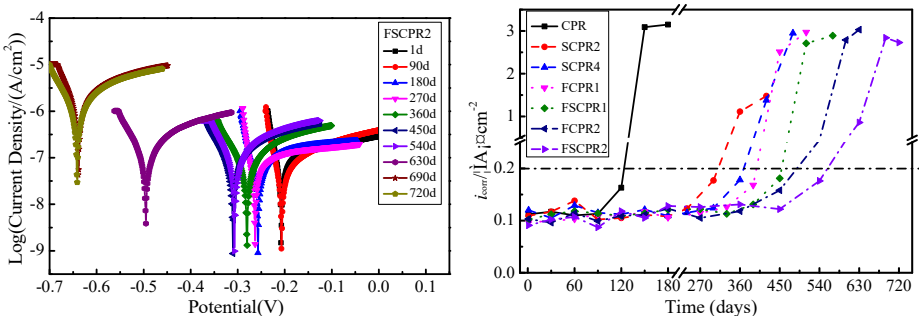

(g) FSCPR2 (h) corrosion current density

Fig. 5 – Tafel polarization and corrosion current density curves of specimens

3.3 Electrochemical impedance spectra (EIS)

In addition to TP, EIS is also an effective method which can be used to evaluate the corrosion behavior of steel bars in concrete under marine environment. As shown in Fig. 6-Fig. 8, in which the Nyquist and Bode curves of the mentioned specimens immersed in seawater are presented. In these Figures, the capacitive arc and phase angle in low-frequency of Nyquist and Bode curves can reflect the corrosion resistance and stability of passive film on the surface of steel bars [37]. Larger capacitive arc diameter and phase angle in low-frequency indicate higher stability of the passive film, namely a better corrosion resistance on the surface of steel bars [38].

It can be observed from Fig. 6 that, there was a large capacitive arc and high phase angle in low-frequency of Nyquist and Bode curves of CPR, and they had basically no changes during the first 90 days of immersion, indicating that the steel bar in CPR was in a passive state. During the immersion days from 90 to 120 of CPR, there occurred an obvious shrink of capacitive arc and decrease in phase angle from around 60° to 40°. Finally, the capacitive arc remarkably shrunk to very small and the phase angle decreased to about 20° on the 150th day, demonstrating the corrosion of steel bars in CPR [39]. Similarly, it also can be found from Figs. 7 and 8 that, the diameters of capacitive arcs in the Nyquist curves' low-frequency of SCPR2, SCPR4, FCPR1, FCPR2 FSCPR1, and FSCPR2 maintained large during the immersion days of 240, 300, 330, 390, 450, and 540, respectively. But their diameters decreased to be very small on the immersion days of 360, 420, 450, 510, 600 and 690, respectively. Correspondingly, on their Bode curves, the phase angles in low-frequency changed from about 60° to 30° at the same period of immersion. The results indicate that the steel bar's surface of these specimens has been keeping passive state and respectively produced corrosion until immersion in the seawater for 360, 420, 450, 510, 600 and 690 days. Thus, the testing results about the corrosion-resistant improving effect of slag/fly ash on steel bar in reinforced concrete observed from EIS is consistent with TP.

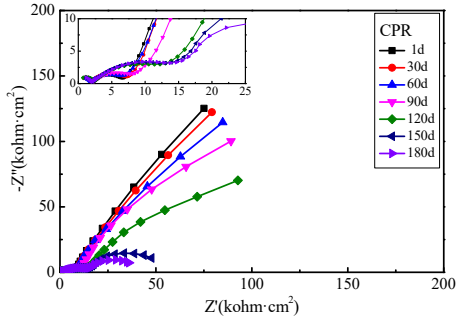

(a) Nyquist

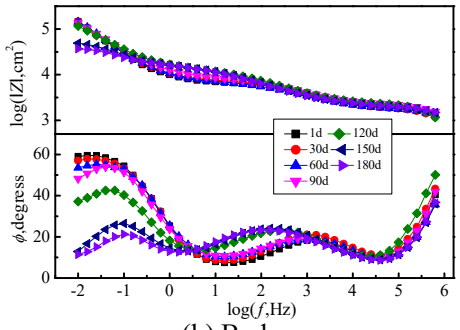

(b) Bode

Fig. 6 – EIS curves of specimen CPR

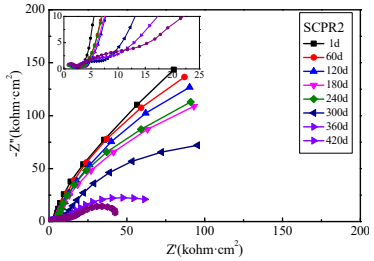

(a) SCPR2

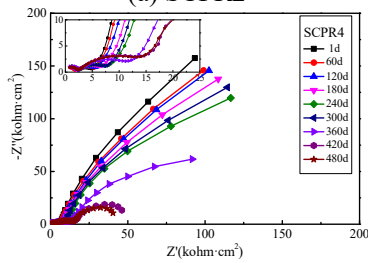

(b) SCPR4

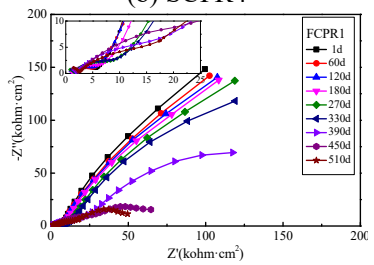

(c) FCPR1

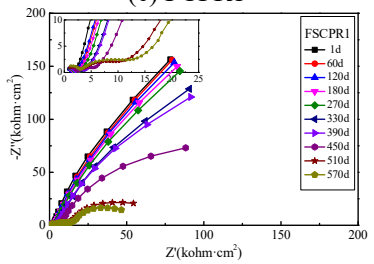

(d) FSCPR1

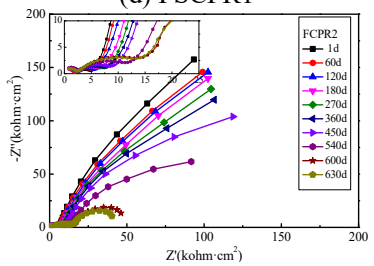

(e) FCPR2

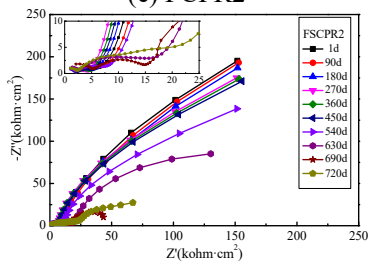

(f) FSCPR2

Fig. 7 – Nyquist curves of specimens

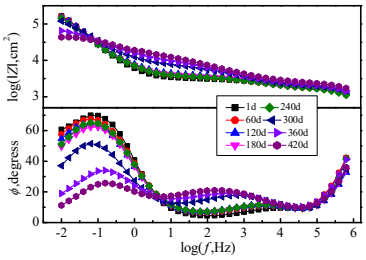

(a) SCPR2

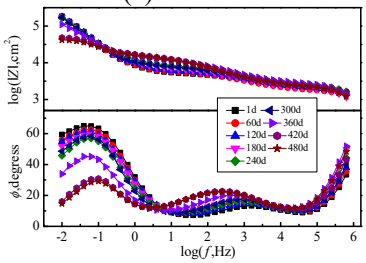

(b) SCPR4

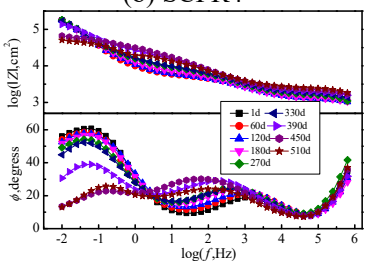

(c) FCPR1

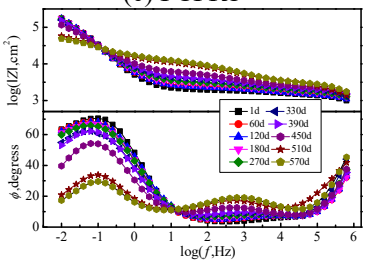

(d) FSCPR1

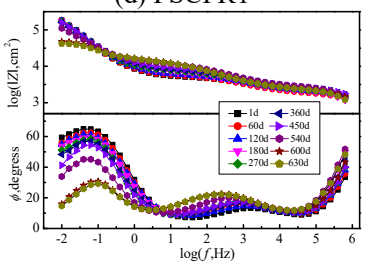

(e) FCPR2

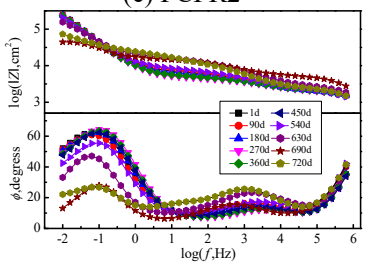

(f) FSCPR2

Fig. 8 – Bode curves of specimens

3.4 EIS data analysis

Based on the structure of the prepared electrochemical specimens and their impedance spectra curves, two equivalent circuits with two-time constants were utilized to fit the EIS data before and after corrosion by ZSimpWin software [40], as demonstrated in Fig. 9. In this figure, R_s, R_c, and R_{ct} represents the resistance of solution, cement paste, and passive film on the steel surface, respectively. C_c and Q_{dl} are the capacitance of double-layer capacitors associated with the solution-cement paste interface and cement paste-steel interface, respectively, meanwhile, W refers to the Warburg impedance caused by diffusion. Both R_{ct} and Q_{dl} can be used to characterize the corrosion behavior of steel surface. It is reported that higher R_{ct} and lower Q_{dl} indicate better corrosion resistance of the steel surface [41]. The fitting results of the electrochemical parameters were shown in Fig. 10 and Fig. 11.

It can be found from Fig. 10 that, the initial R_{ct} of CPR, SCPR2, SCPR4, FCPR1, FCPR2 FSCPR1, and FSCPR2 was respectively 521.4, 611.8, 689.1, 565.4, 647.8, 587.8, and 583.0 kΩ·cm^2. Also, their R_{ct} basically had no change during the initial state of immersion. However, after a period of immersion, their R_{ct} obviously decreased to very small within short time, such as 14.6, 13.4, and 21.0 kΩ·cm^2 for specimens of CPR, SCPR2, and SCPR4, respectively. This process indicated that the passive film on the steel surface was generally weakened and finally destroyed by the seawater environment. The difference was that specimens with different contents of slag and fly ash showed a different corrosion time, which demonstrated that the equivalent replacement of cement with slag can slow down the depassivation of steel bar in concrete, and improve the corrosion resistance of reinforced concrete in chloride environment.

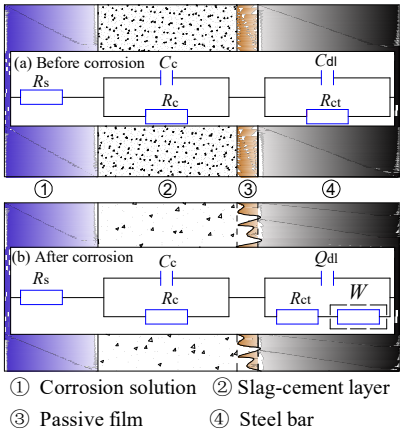

Fig. 9 – Equivalent circuits of working electrode

In addition, the double-layer capacitor, Q_{dl}, can also characterize the corrosion degree of steel surface [42]. It was reported that a higher corrosion degree produced more deviation of the Q_{dl} from the ideal capacitor, indicating a higher surface roughness of steel surfaces [43]. According to Vedalakshmi's [38] point of view, the surface of steel is in a passive state when the Q_{dl} is less than 100 μF·cm^{-2}, otherwise it is in depassivated state. As displayed in Fig. 11, the Q_{dl} of CPR, SCPR2, SCPR4, FCPR1, FCPR2 FSCPR1, and FSCPR2 all increased to more than 100 μF·cm^{-2} after immersion in the seawater for a period of time. The results were consistent with the testing result of R_{ct}, proving the gradually corrosion of steel and the positively improving effect of slag and fly ash on corrosion resistance of steel in concrete. Besides, the non-uniform changes of the mentioned time-varying OCP, TP, and EIS curves indicate that the corrosion of reinforced concrete in the marine environment does not occur at a uniform rate, but first maintains a long-term uncorroded state, and develops rapidly after pitting corrosion occurred.

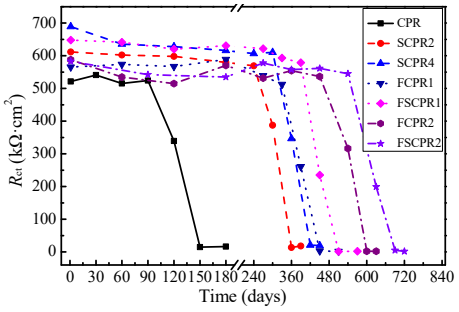

Fig. 10 – Time-varying curves of Rct

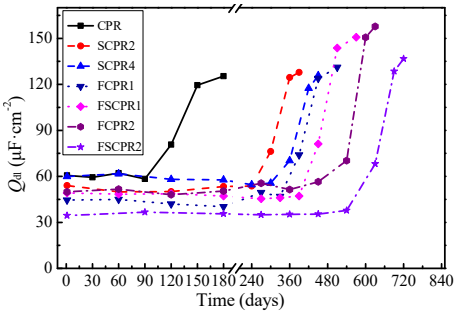

Fig. 11 – Time-varying curves of Q_{dl}

3.5 Micromorphology

In order to clarify the corrosion of steel bars in cement paste under seawater environment, specimens of CPR, SCPR2 and SCPR4 were broken to prepare the SEM/EDS samples after electrochemical tests. These samples were utilized to observe the morphology and composition of the cement paste-steel interface, as shown in Figs. 12~17. It can be observed from the surface morphology on steel bar of CPR, SCPR2 and SCPR4

in Fig. 12 that, there were rusty spot at the zone of A1, smooth surface at the zone of A2, and demarcation line between them, indicating that an obvious corrosion has occurred on the surface of steel bar. Additionally, the zones of A1 and A2 were further enlarged to analyze their microstructure and elemental composition. As shown in Fig. 13, the loose and pit-shaped corrosion products can be observed at the zone of A1, and the elemental compositions at its spot S1 tested by EDS were mainly iron and oxygen with little amounts of carbon and calcium. Comparatively, it can be found from Fig. 14 that, there were some scratches with no corrosion products at the zone of A2, and the elemental compositions at its spot S2 is 93.15% iron and 0.61% carbon, which is like the elemental composition of unoxidized steel [44]. The decrease in iron content and increase in oxygen content indicate the formation of rust on the surface of steel [45,46], thus demonstrating the corrosion of steel bars in CPR, SCPR2 and SCPR4.

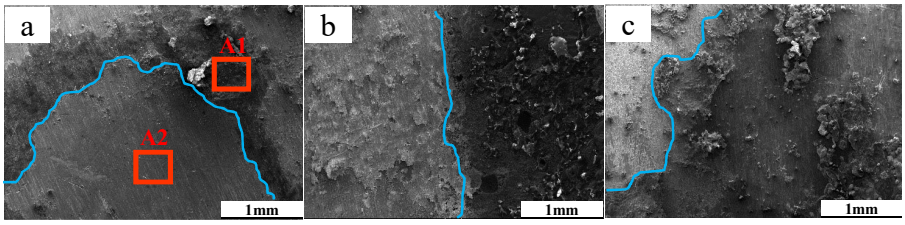

Fig. 12 – Surface morphology of steel: (a) CPR, (b) SCPR2 and (c) SCPR4

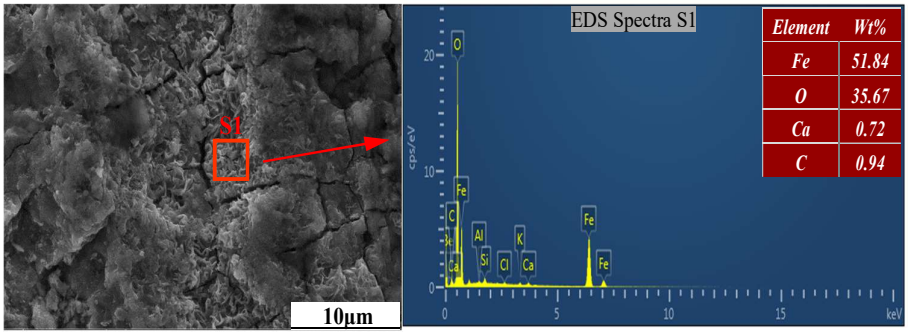

Fig. 13 – Microstructure morphology and elemental composition at area A1

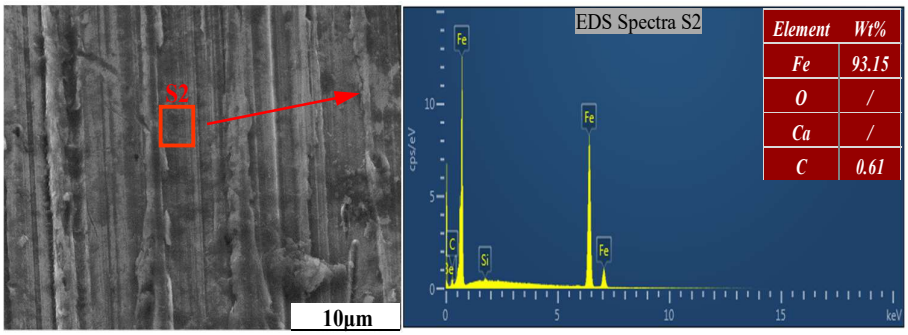

Fig. 14 – Microstructure morphology and elemental composition at area A2

Fig. 15 presents the surface morphology of inner cement paste of CPR, SCPR2 and SCPR4 after the electrochemical tests. Two different zones, corroded zone and uncorroded zone, can be clearly observed in this figure of the three cement paste samples. Furthermore, the demarcation line in Fig. 15 (a) was enlarged to analyze its microstructure and elemental composition, as shown in Figs. 16 and 17. In Fig. 16, the loose and flocculent C-S-H gel, flake-structure rust with cracks, and demarcation line of them can be observed. Meanwhile, the elemental compositions of spots S3, S4 and, S5 were found to be different. The elements at spot S3 in Fig. 17(a) were mainly iron and oxygen, indicating that the formed rust was attached to the surface of cement paste. The elements at spot S5 in Fig. 17(c) were mainly oxygen and calcium, which is consistent with the elemental compositions of cement hydration products [47,48]. But for elemental composition at spot S4 in Fig. 17(b), iron, oxygen, and calcium all

became primary element with content over 20%, indicating the exist of demarcation line which contained both rusts and cement hydration products. These results further demonstrate the corrosion on the steel bar surface of CPR, SCPR2 and SCPR4.

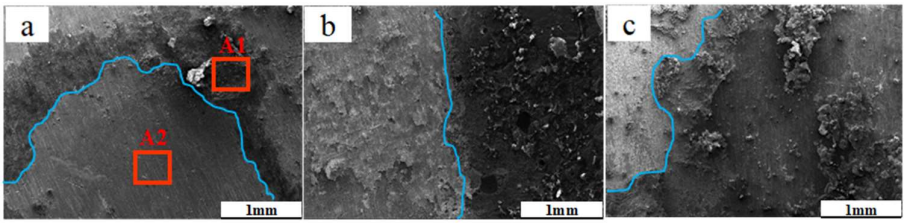

Fig. 15 – Surface morphology of cement paste layers: (a) CPR, (b) SCPR2, (c) SCPR4

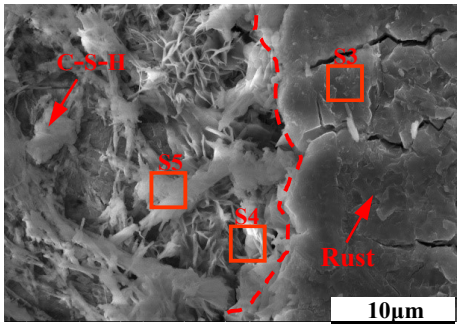

Fig. 16 – Microstructure morphology of demarcation area

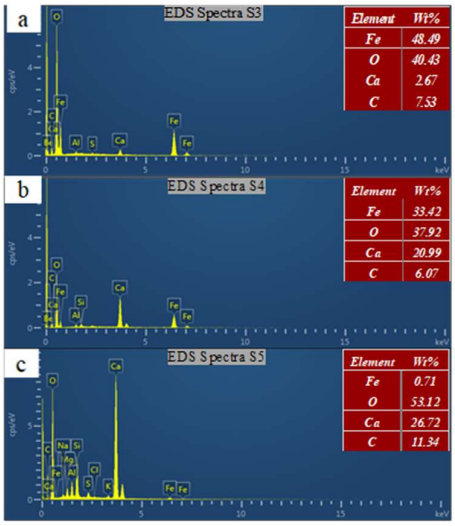

Fig. 17 – Elemental composition of demarcation area: (a) S3, (b) S4, (c) S5

3.6 Phase composition

In order to investigate the effect of slag and fly ash on the corrosion behavior of steel bars in cement paste under chloride environment, the phase compositions of the cement paste powder samples of CPR, SCPR2, SCPR4, FCPR1, FCPR2, FSCPR1, and FSCPR2 were analyzed by XRD, as illustrated in Fig. 18. It can be observed from this figure that, the primary phase compositions of sample CPR were $Ca(OH)_2$, $Ca_{1.5}SiO_{3.5}{\cdot}xH_2O$ and $Ca_5Si_6O_{16}(OH)_2$. In contrast, the phase compositions of samples added with slag and fly ash contained not only $Ca(OH)_2$ and C-S-H gels but also Friedel's salt and $CaAl_2Si_2O_8{\cdot}4H_2O$. Furthermore, by comparing the diffraction peaks which can reflect the relative content of the phase in Fig. 18., it can be found that the contents of C-S-H gels, Friedel's salt and $CaAl_2Si_2O_8{\cdot}4H_2O$ increased with the contents of slag and fly ash, while the content of $Ca(OH)_2$ appeared to be a decrease. One one hand, this is because the pozzolanic reaction of slag and fly ash consumed $Ca(OH)_2$ to produce C-S-H gels [49]. On the other hand, the content of active Al_2O_3 in slag and fly ash is more than that in cement, thereafter increasing the content of Friedel's salt which is produced by the hydration of C_3A [50]. It was reported that C-S-H gels played a role in physical adsorption of chloride ion, while C_3A can react with chloride ion to form Friedel's salt which chemically combined chloride ion [51,52]. Thus, replacing cement with slag and fly ash can promote the physical adsorption and chemical binding capacity of concrete to free chloride ions, thereafter slowing down the chloride diffusion in concrete and improving the corrosion resistance of reinforced concrete in chloride environment.

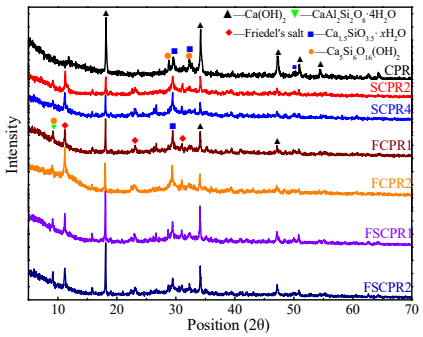

Fig. 18 – XRD patterns of CPR, SCPR2, SCPR4, FCPR1, FCPR2, FSCPR1, and FSCPR2

4. Conclusions

In this study, the effect of slag and fly ash on the

corrosion behavior of steel bars in concrete under marine environment was investigated by performing a series corrosion experiments of cement paste specimens with different contents of slay and fly ash under seawater. In the investigation, the corrosion behavior of specimens was electrochemically monitored by open-circuit potential (OCP), Tafel polarization (TP) and electrochemical impedance spectra (EIS), meanwhile, SEM/EDS and XRD were applied to microscopically analyze the specimen's microstructure evolution. The following conclusions can be drawn according to the test results and analysis:

(1) The steel bar of specimens with 100% cement, 20% slag, 40% slag, 10% fly ash, 20% fly ash, 10% slag + 10% fly ash, and 20% slay + 20% fly ash corroded under seawater on the 150^{th}, 360^{th}, 420^{th}, 450^{th}, 510^{th}, 600^{th} and 690^{th} day, respectively, indicating that the replacement of cement with slag and fly ash can delay the initial corrosion time and improve the corrosion resistance of reinforced concrete in marine environment.

(2) Compared to slag, the equal replacing content of fly ash can contribute to a better improving effect on the corrosion resistance of reinforced concrete in marine environment. In this study, content of 20% slag + 20% fly ash replacement of cement led to the best improving effect of corrosion resistance.

(3) The corrosion of reinforced bars in concrete under marine environment does not occur at a uniform rate, but first maintains a long-term uncorroded state, and develops rapidly after pitting corrosion occurs.

(4) Adding slag and fly ash caused a decrease of $Ca(OH)_2$ as well as an increase of C-S-H gel and Friedel's salt in the phase composition of concrete, which can improve the chloride-solidification ability and slow down the chloride diffusion in concrete by physical adsorption and chemical binding, and thereafter promote the corrosion resistance of reinforced concrete in the marine environment.

Acknowledgements

The study of this paper is financially supported by the National Natural Science Foundation of China (51778297, 52078252)

References

[1] Laurens, S., Hénocq, P., Rouleau, N., Deby, F., Samson, E., Marchand, J., and Bissonnette, B., (2016). Steady-state polarization response of chloride-induced macrocell corrosion systems in steel reinforced concrete—numerical and experimental investigations, *Cement and Concrete Research*, 79, 272–290.

[2] Shi, X., Xie, N., Fortune, K., and Gong, J., (2012). Durability of steel reinforced concrete in chloride environments: An overview, *Construction and Building Materials*, 30, 125–138.

[3] Zheng, H., Dai, J.-G., Hou, L., Meng, G., Poon, C.S., and Li, W., (2020). Enhanced passivation of galvanized steel bars in nano-silica modified cement mortars, *Cement and Concrete Composites*, 111, 103626.

[4] Zheng, L., Wu, H., Zhang, H., Duan, H., Wang, J., Jiang, W., Dong, B., Liu, G., Zuo, J., and Song, Q., (2017). Characterizing the generation and flows of construction and demolition waste in China, *Construction and Building Materials*, 136, 405–413. https://doi.org/10.1016/j.conbuildmat.2017.01.055.

[5] Kenny, A. and Katz, A., (2020). Steel-concrete interface influence on chloride threshold for corrosion–Empirical reinforcement to theory, *Construction and Building Materials*, 244, 118376.

[6] Li, C., Jiang, L., and Li, S., (2020). Effect of limestone powder addition on threshold chloride concentration for steel corrosion in reinforced concrete, *Cement and Concrete Research*, 131, 106018.

[7] Wu, Z., Yu, H., Ma, H., Zhang, J., Da, B., and Zhu, H., (2020). Rebar corrosion in coral aggregate concrete: determination of chloride threshold by LPR, *Corrosion Science*, 163, 108238.

[8] Yang, C., Li, L., and Li, J., (2020). Service life of reinforced concrete seawalls suffering from chloride attack: Theoretical modelling and analysis, *Construction and Building Materials*, 263, 120172.

[9] Li, J. and Shao, W., (2014). The effect of chloride binding on the predicted service life of RC pipe piles exposed to marine environments, *Ocean Engineering*, 88, 55–62.

[10] Torbati-Sarraf, H. and Poursaee, A., (2018). Corrosion of coupled steels with different microstructures in concrete environment, *Construction and Building Materials*, 167, 680–687.

[11] Tang, S.W., Yao, Y., Andrade, C., and Li, Z.J., (2015). Recent durability studies on concrete structure, *Cement and Concrete Research*, 78, 143–154.

[12] Ahmed, A., Guo, S., Zhang, Z., Shi, C., and Zhu, D., (2020). A review on durability of fiber reinforced polymer (FRP) bars reinforced seawater sea sand concrete, *Construction and Building Materials*, 256, 119484.

[13] Herath, C., Gunasekara, C., Law, D.W., and Setunge, S., (2020). Performance of high volume fly ash concrete incorporating additives: A

systematic literature review, *Construction and Building Materials*, 258, 120606.

[14] Amran, M., Debbarma, S., and Ozbakkaloglu, T., (2021). Fly ash-based eco-friendly geopolymer concrete: A critical review of the long-term durability properties, *Construction and Building Materials*, 270, 121857.

[15] Hassan, A., Arif, M., and Shariq, M., (2019). Use of geopolymer concrete for a cleaner and sustainable environment–A review of mechanical properties and microstructure, *Journal of Cleaner Production*, 223, 704–728.

[16] Ogirigbo, O.R. and Black, L., (2016). Influence of slag composition and temperature on the hydration and microstructure of slag blended cements, *Construction and Building Materials*, 126, 496–507.

[17] Hu, X., Shi, C., Shi, Z., and Zhang, L., (2019). Compressive strength, pore structure and chloride transport properties of alkali-activated slag/fly ash mortars, *Cement and Concrete Composites*, 104, 103392.

[18] Shi, J., Ming, J., and Sun, W., (2018). Electrochemical behaviour of a novel alloy steel in alkali-activated slag mortars, *Cement and Concrete Composites*, 92, 110–124.

[19] Jau, W.-C. and Tsay, D.-S., (1998). A study of the basic engineering properties of slag cement concrete and its resistance to seawater corrosion, *Cement and Concrete Research*, 28, 1363–1371.

[20] Topçu, İ.B. and Boğa, A.R., (2010). Effect of ground granulate blast-furnace slag on corrosion performance of steel embedded in concrete, *Materials & Design*, 31, 3358–3365.

[21] Mangat, P.S. and Molloy, B.T., (1991). Influence of PFA, slag and microsilica on chloride induced corrosion of reinforcement in concrete, *Cement and Concrete Research*, 21, 819–834.

[22] Tsouli, S., Lekatou, A.G., Kleftakis, S., Matikas, T.E., and Dalla, P.T., (2018). Corrosion behavior of 304L stainless steel concrete reinforcement in acid rain using fly ash as corrosion inhibitor, *Procedia Structural Integrity*, 10, 41–48.

[23] Tittarelli, F., Mobili, A., and Bellezze, T., The Effect of Fly Ash on the Corrosion Behaviour of Galvanised Steel Rebarsin Concrete, in: IOP Conf. Ser. Mater. Sci. Eng., IOP Publishing, 2017: p. 12107.

[24] Uthaman, S., George, R.P., Vishwakarma, V., Harilal, M., and Philip, J., (2019). Enhanced seawater corrosion resistance of reinforcement in nanophase modified fly ash concrete, *Construction and Building Materials*, 221, 232–243.

[25] Hao, W., Liu, Z., Wu, W., Li, X., Du, C., and Zhang, D., (2018). Electrochemical characterization and stress corrosion cracking of E690 high strength steel in wet-dry cyclic marine environments, *Materials Science and Engineering: A*, 710, 318–328.

[26] Luo, H., Su, H., Li, B., and Ying, G., (2018). Electrochemical and passive behaviour of tin alloyed ferritic stainless steel in concrete environment, *Applied Surface Science*, 439, 232–239.

[27] Goyal, A., Pouya, H.S., Ganjian, E., Olubanwo, A.O., and Khorami, M., (2019). Predicting the corrosion rate of steel in cathodically protected concrete using potential shift, *Construction and Building Materials*, 194, 344–349.

[28] Subramaniam, K. V and Bi, M., (2010). Investigation of steel corrosion in cracked concrete: Evaluation of macrocell and microcell rates using Tafel polarization response, *Corrosion Science*, 52, 2725–2735.

[29] Ribeiro, D. V and Abrantes, J.C.C., (2016). Application of electrochemical impedance spectroscopy (EIS) to monitor the corrosion of reinforced concrete: A new approach, *Construction and Building Materials*, 111, 98–104.

[30] Mohamed, N., Boulfiza, M., and Evitts, R., (2013). Corrosion of carbon steel and corrosion-resistant rebars in concrete structures under chloride ion attack, *Journal of Materials Engineering and Performance*, 22, 787–795.

[31] Amin, M.A., Khaled, K.F., and Fadl-Allah, S.A., (2010). Testing validity of the Tafel extrapolation method for monitoring corrosion of cold rolled steel in HCl solutions–experimental and theoretical studies, *Corrosion Science*, 52, 140–151.

[32] Lee, S.T. and Hooton, R.D., (2016). Influence of limestone addition on the performance of cement mortars and pastes exposed to a cold sodium sulfate solution, *Journal of Testing and Evaluation*, 44, 414–423.

[33] G102-89, A., (1999). Standard practice for calculation of corrosion rates and related information from electrochemical measurements, *Reapproved 1999*,.

[34] Luo, H., Su, H., Dong, C., Xiao, K., and Li, X., (2015). Electrochemical and passivation behavior investigation of ferritic stainless steel in alkaline environment, *Construction and Building Materials*, 96, 502–507.

[35] Song, H.-W. and Saraswathy, V., (2007). Corrosion monitoring of reinforced concrete structures-A, *Int. J. Electrochem. Sci*, 2, 1–28.

[36] Clear, K.C., (1989). Measuring rate of corrosion of steel in field concrete structures, *Transportation Research Record*,.

[37] Koleva, D.A., (2011). Electrochemical behavior of corroded and protected construction steel in cement extract, *Materials and Corrosion*, 62, 240–251.

[38] Vedalakshmi, R. and Palaniswamy, N., (2010). Analysis of the electrochemical phenomenon at the rebar–concrete interface using the electrochemical impedance spectroscopic

technique, *Magazine of Concrete Research*, 62, 177–189.

[39] Hu, X., Shi, C., Liu, X., Zhang, J., and De Schutter, G., (2019). A review on microstructural characterization of cement-based materials by AC impedance spectroscopy, *Cement and Concrete Composites*, 100, 1–14.

[40] Tian, Y., Dong, C., Cheng, X., Wan, Y., Wang, G., Xiao, K., and Li, X., (2017). The micro-solution electrochemical method to evaluate rebar corrosion in reinforced concrete structures, *Construction and Building Materials*, 151, 607–614.

[41] Lee, H.-S., Yang, H.-M., Singh, J.K., Prasad, S.K., and Yoo, B., (2018). Corrosion mitigation of steel rebars in chloride contaminated concrete pore solution using inhibitor: An electrochemical investigation, *Construction and Building Materials*, 173, 443–451.

[42] Terbouche, A., Lameche, S., Ait-Ramdane-Terbouche, C., Guerniche, D., Lerari, D., Bachari, K., and Hauchard, D., (2016). A new electrochemical sensor based on carbon paste electrode/Ru (III) complex for determination of nitrite: Electrochemical impedance and cyclic voltammetry measurements, *Measurement*, 92, 524–533.

[43] Cruz, J., Pandiyan, T., and Garcia-Ochoa, E., (2005). A new inhibitor for mild carbon steel: electrochemical and DFT studies, *Journal of Electroanalytical Chemistry*, 583, 8–16.

[44] Refait, P., Grolleau, A.-M., Jeannin, M., François, E., and Sabot, R., (2018). Corrosion of mild steel at the seawater/sediments interface: Mechanisms and kinetics, *Corrosion Science*, 130, 76–84.

[45] Jiang, S., Chai, F., Su, H., and Yang, C., (2017). Influence of chromium on the flow-accelerated corrosion behavior of low alloy steels in 3.5% NaCl solution, *Corrosion Science*, 123, 217–227.

[46] Wang, Y., Cheng, G., Wu, W., and Li, Y., (2018). Role of inclusions in the pitting initiation of pipeline steel and the effect of electron irradiation in SEM, *Corrosion Science*, 130, 252–260.

[47] Tang, Y.-J., Zuo, X.-B., He, S.-L., Ayinde, O., and Yin, G.-J., (2016). Influence of slag content and water-binder ratio on leaching behavior of cement pastes, *Construction and Building Materials*, 129, 61–69.

[48] Lemonis, N., Tsakiridis, P.E., Katsiotis, N.S., Antiohos, S., Papageorgiou, D., Katsiotis, M.S., and Beazi-Katsioti, M., (2015). Hydration study of ternary blended cements containing ferronickel slag and natural pozzolan, *Construction and Building Materials*, 81, 130–139.

[49] Ustabaş, İ. and Kaya, A., (2018). Comparing the pozzolanic activity properties of obsidian to those of fly ash and blast furnace slag, *Construction and Building Materials*, 164, 297–307.

[50] Talero, R., (2012). Synergic effect of Friedel's salt from pozzolan and from OPC co-precipitating in a chloride solution, *Construction and Building Materials*, 33, 164–180.

[51] Zhou, Y., Hou, D., Jiang, J., Liu, L., She, W., and Yu, J., (2018). Experimental and molecular dynamics studies on the transport and adsorption of chloride ions in the nano-pores of calcium silicate phase: the influence of calcium to silicate ratios, *Microporous and Mesoporous Materials*, 255, 23–35.

[52] Gbozee, M., Zheng, K., He, F., and Zeng, X., (2018). The influence of aluminum from metakaolin on chemical binding of chloride ions in hydrated cement pastes, *Applied Clay Science*, 158, 186–194.